



MAXI J1848-015: The First Detection of Relativistically Moving Outflows from a Globular Cluster X-ray Binary

A Bahramian, E Tremou, A.J Tetarenko, J.C.A Miller-Jones, R.P Fender, Stéphane Corbel, D.R.A Williams, J Strader, F Carotenuto, R Salinas, et al.

► To cite this version:

A Bahramian, E Tremou, A.J Tetarenko, J.C.A Miller-Jones, R.P Fender, et al.. MAXI J1848-015: The First Detection of Relativistically Moving Outflows from a Globular Cluster X-ray Binary. *Astrophys.J.Lett.*, 2023, 948 (1), pp.L7. 10.3847/2041-8213/accde1 . hal-04096361

HAL Id: hal-04096361

<https://hal.science/hal-04096361>

Submitted on 13 May 2023

HAL is a multi-disciplinary open access archive for the deposit and dissemination of scientific research documents, whether they are published or not. The documents may come from teaching and research institutions in France or abroad, or from public or private research centers.

L'archive ouverte pluridisciplinaire **HAL**, est destinée au dépôt et à la diffusion de documents scientifiques de niveau recherche, publiés ou non, émanant des établissements d'enseignement et de recherche français ou étrangers, des laboratoires publics ou privés.



Distributed under a Creative Commons Attribution 4.0 International License



MAXI J1848-015: The First Detection of Relativistically Moving Outflows from a Globular Cluster X-Ray Binary

A. Bahramian¹ , E. Tremou² , A. J. Tetarenko^{3,4,15} , J. C. A. Miller-Jones¹ , R. P. Fender^{5,6} , S. Corbel^{7,8} , D. R. A. Williams⁹ , J. Strader¹⁰ , F. Carotenuto⁵ , R. Salinas¹¹ , J. A. Kennea¹² , S. E. Motta¹³ , P. A. Woudt⁶ , J. H. Matthews⁵ , and T. D. Russell¹⁴

¹ International Centre for Radio Astronomy Research - Curtin University, GPO Box U1987, Perth, WA 6845, Australia; arash.bahramian@curtin.edu.au

² National Radio Astronomy Observatory, Socorro, NM 87801 USA

³ Department of Physics and Astronomy, Texas Tech University, Lubbock, TX 79409-1051, USA

⁴ East Asian Observatory, 660 N. A'ohōkū Place, University Park, Hilo, HI 96720, USA

⁵ Astrophysics, Department of Physics, University of Oxford, Keble Road, Oxford OX1 3RH, UK

⁶ Department of Astronomy, University of Cape Town, Private Bag X3, Rondebosch 7701, South Africa

⁷ Université Paris Cité and Université Paris Saclay, CEA, CNRS, AIM, F-91190 Gif-sur-Yvette, France

⁸ ORN, Observatoire de Paris, Université PSL, Université Orléans, CNRS, F-18330 Nançay, France

⁹ Jodrell Bank Centre for Astrophysics, School of Physics and Astronomy, The University of Manchester, Manchester M13 9PL, UK

¹⁰ Center for Data Intensive and Time Domain Astronomy, Department of Physics and Astronomy, Michigan State University, East Lansing, MI 48824, USA

¹¹ Gemini Observatory/NSF's NOIRLab, Casilla 603, La Serena, Chile

¹² Department of Astronomy and Astrophysics, The Pennsylvania State University, 525 Davey Lab, University Park, PA 16802, USA

¹³ Istituto Nazionale di Astrofisica, Osservatorio Astronomico di Brera, via E. Bianchi 46, I-23807 Merate (LC), Italy

¹⁴ INAF, Istituto di Astrofisica Spaziale e Fisica Cosmica, Via U. La Malfa 153, I-90146 Palermo, Italy

Received 2023 January 30; revised 2023 April 4; accepted 2023 April 18; published 2023 April 28

Abstract

Over the past decade, observations of relativistic outflows from outbursting X-ray binaries in the Galactic field have grown significantly. In this work, we present the first detection of moving and decelerating radio-emitting outflows from an X-ray binary in a globular cluster. MAXI J1848–015 is a recently discovered transient X-ray binary in the direction of the globular cluster GLIMPSE-C01. Using observations from the Karl G. Jansky Very Large Array, and a monitoring campaign with the MeerKAT observatory for 500 days, we model the motion of the outflows. This represents some of the most intensive, long-term coverage of relativistically moving X-ray binary outflows to date. We use the proper motions of the outflows from MAXI J1848–015 to constrain the component of the intrinsic jet speed along the line of sight, $\beta_{\text{int}} \cos \theta_{\text{ejection}}$, to be 0.19 ± 0.02 . Assuming it is located in GLIMPSE-C01, at 3.4 kpc, we determine the intrinsic jet speed, $\beta_{\text{int}} = 0.79 \pm 0.07$, and the inclination angle to the line of sight, $\theta_{\text{ejection}} = 76^\circ \pm 2^\circ$. This makes the outflows from MAXI J1848–015 somewhat slower than those seen from many other known X-ray binaries. We also constrain the maximum distance to MAXI J1848–015 to be 4.3 kpc. Finally, we discuss the implications of our findings for the nature of the compact object in this system, finding that a black hole primary is a viable (but as-of-yet unconfirmed) explanation for the observed properties of MAXI J1848–015. If future data and/or analysis provide more conclusive evidence that MAXI J1848–015 indeed hosts a black hole, it would be the first black hole X-ray binary in outburst identified in a Galactic globular cluster.

Unified Astronomy Thesaurus concepts: Radio jets (1347); Low-mass x-ray binary stars (939); Neutron stars (1108); Black holes (162); Stellar accretion (1578); Globular star clusters (656)

1. Introduction

On 2020 December 20, the Monitor of All-sky X-ray Image (MAXI) mission detected a bright outburst from the direction of the globular cluster GLIMPSE-C01 (Takagi et al. 2020). At the time, the source (named MAXI J1848–015) was located in the Sun-constraint zone for most other X-ray observatories. However, follow-up observations by the Nuclear Spectroscopic Telescope Array (NuSTAR) improved on localization and found indications of spectral evolution (Pike et al. 2020; Mihara et al. 2021). A follow-up observation by the X-ray Telescope (XRT) on board the Neil Gehrels Swift Observatory (Swift/XRT) on 2021 February 21 found MAXI J1848–015

still in outburst and localized it to the core of GLIMPSE-C01, suggesting that this outburst may come from a previously undetected X-ray binary (XRB) in this star cluster (Kennea et al. 2021). A further follow-up observation by the Chandra observatory provided improved constraints on the location (Chakrabarty et al. 2021), while inspection of archival Chandra data provided a deep upper limit on the quiescent X-ray luminosity of $\leq 3.3 \times 10^{30} \text{ erg s}^{-1}$ in the 0.5–10 keV band (Hare et al. 2021).

In contrast with the Galactic field, globular clusters are known to contain an overabundance of XRBs (Clark 1975). This is generally attributed to dynamical formation of these systems through encounters as opposed to canonical binary evolution (Fabian et al. 1975; Sutantyo 1975; Hills 1976). Observational evidence in support of this overabundance has been discussed both for Galactic (Heinke et al. 2003; Pooley et al. 2003; Bahramian et al. 2013) and extragalactic (Sarazin et al. 2003; Kundu et al. 2007; Kundu & Zepf 2007) clusters.

GLIMPSE-C01 is a star cluster located 0.1° away from the Galactic plane (Kobulnicky et al. 2005). It is at an estimated

¹⁵ NASA Einstein Fellow.



Table 1
VLA and MeerKAT Observations of MAXI J1848–015 Discussed in This Work

Date	MJD	Exposure	Date	MJD	Exposure	Date	MJD	Exposure
2021-02-27	59,272.522	4 hr	2021-07-04	59,399.901	15 minutes	2021-12-18	59,566.443	15 minutes
2021-03-06	59,279.221	15 minutes	2021-07-12	59,407.019	15 minutes	2022-01-03	59,582.381	15 minutes
2021-03-13	59,286.110	15 minutes	2021-07-26	59,421.702	15 minutes	2022-01-16	59,595.315	15 minutes
2021-03-20	59,293.150	15 minutes	2021-07-31	59,426.898	15 minutes	2022-01-29	59,608.433	15 minutes
2021-03-28	59,301.290	15 minutes	2021-08-07	59,433.909	15 minutes	2022-02-14	59,624.221	15 minutes
2021-04-05	59,309.185	15 minutes	2021-08-15	59,441.921	15 minutes	2022-02-27	59,637.360	15 minutes
2021-04-10	59,314.093	15 minutes	2021-08-22	59,448.673	15 minutes	2022-03-16	59,654.239	15 minutes
2021-04-19	59,323.003	15 minutes	2021-08-28	59,454.676	15 minutes	2022-03-28	59,666.106	15 minutes
2021-04-24	59,328.024	15 minutes	2021-09-05	59,462.751	15 minutes	2022-04-10	59,679.088	15 minutes
2021-05-01	59,335.077	15 minutes	2021-09-13	59,470.646	15 minutes	2022-04-25	59,694.105	15 minutes
2021-05-07	59,341.109	15 minutes	2021-09-20	59,477.678	15 minutes	2022-05-07	59,706.052	15 minutes
2021-05-15	59,349.920	15 minutes	2021-09-27	59,484.594	15 minutes	2022-05-23	59,722.951	15 minutes
2021-05-22	59,356.032	15 minutes	2021-10-04	59,491.658	15 minutes	2022-06-03	59,733.961	15 minutes
2021-05-27	59,361.965	15 minutes	2021-10-17	59,504.508	15 minutes	2022-06-17	59,747.929	15 minutes
2021-06-05	59,370.907	15 minutes	2021-10-23	59,510.519	15 minutes	2022-07-03	59,763.962	15 minutes
2021-06-12	59,377.956	15 minutes	2021-11-08	59,526.638	15 minutes	2022-07-15	59,775.849	15 minutes
2021-06-19	59,384.910	15 minutes	2021-11-19	59,537.677	15 minutes	2022-07-30	59,790.750	15 minutes
2021-06-27	59,392.034	15 minutes	2021-12-04	59,552.425	15 minutes			

Note. MJD column represents the Modified Julian Date at the start of the observation. The VLA X-band observation (performed on 2021 February 27) was centered at 10 GHz. The MeerKAT *L*-band observations were all centered at 1.284 GHz.

distance of 3.4 kpc (Hare et al. 2018) from us, corresponding to a distance of 6 pc from the Galactic midplane. This highly extinguished cluster ($E(B - V) \approx 4.85$; Harris 1996, version 2010) has been suspected to be a globular cluster (possibly passing through the Galactic plane or corotating with the Galactic disk; R. Salinas et al. 2023, in preparation) due to properties including its well-populated giant branch—indicating an abundance of old low-mass giants, as opposed to young supergiants, and high stellar density in the core—hinting at mass segregation, a well-known property of old, relaxed globular clusters (Ivanov et al. 2005; Kobulnicky et al. 2005; Davidge et al. 2016). In the X-rays, GLIMPSE-C01 is known to host more than a dozen X-ray sources (Pooley et al. 2007; Hare et al. 2018).

In this work, we report the detection of radio outflows moving away from the core of MAXI J1848–015, observed by the Karl G. Jansky Very Large Array (VLA) and MeerKAT. We also detect clear deceleration of these outflows as they move through the interstellar medium (ISM). Moving outflows have been observed in a number of black hole XRBs (Mirabel & Rodríguez 1994; Hjellming & Rupen 1995; Fomalont et al. 2001a; Corbel et al. 2002, 2005; Yang et al. 2011; Martí et al. 2017; Rushton et al. 2017; Miller-Jones et al. 2019; Bright et al. 2020), and with the emergence of facilities such as MeerKAT, decelerating outflows interacting with the ISM have now been seen in several XRBs at different distances, opening angles and times (up to months or years). However, MAXI J1848–015 is the first XRB in a globular cluster to be observed exhibiting such outflows. Furthermore, the outflows from MAXI J1848–015 show some of the most persistent radio emission from relativistically moving XRB outflows observed to date (see also XTE J1550–564, XTE J1748–288, MAXI J1535–571, MAXI J1820+070, and MAXI J1348–630; Corbel et al. 2001; Brocksopp et al. 2007; Russell et al. 2019; Bright et al. 2020; Carotenuto et al. 2021). In Section 2 we describe the data presented in this work and details of the data processing. In Section 3, we determine the location of a potential compact radio core and measure the motion of the moving outflows, and finally in Section 4 we

explore the implications of our findings, considering the host environment and making comparisons with other, similar, systems. The outflows were also independently identified in data from the VLA Low-band Ionosphere and Transient Experiment (VLITE) at 340 MHz (W. Peters et al. 2023, in preparation).

2. Data and Reduction

Soon after the localization of MAXI J1848–015 to the core of GLIMPSE-C01, we began an intense monitoring campaign in the radio band to constrain its nature and study the outflows. The observations analyzed in this work are summarized in Table 1.

2.1. VLA

MAXI J1848–015 was observed with the VLA (Project Code: 21A–400) on 2021 February 27 (MJD 59,272), for a total on-source observation time of ~ 88 minutes. During our observations, the array was in its most extended A-configuration, observing in the 8–12 GHz band, with the 3-bit samplers. The correlator was set up to generate two basebands, each with 16 spectral windows comprising 64 2 MHz channels, giving a total bandwidth of 2.048 GHz per baseband. We reduced and imaged the data within the Common Astronomy Software Application package (CASA, version 5.4; THE CASA TEAM et al. 2022), using standard procedures outlined in the CASA Guides¹⁶ for VLA data reduction (i.e., a priori flagging, setting the flux density scale, initial phase calibration, solving for antenna-based delays, bandpass calibration, gain calibration, scaling the amplitude gains, and final target flagging). We used 3C286 (J1331+3030) as a flux/bandpass calibrator and J1851+0035 as a phase calibrator. We flagged short spacings (< 400 k λ) for J1851+0035, as the VLA calibrator catalog¹⁷ indicates it is extended at these short spacings. To image the target source, we used

¹⁶ https://casaguides.nrao.edu/index.php/Karl_G._Jansky_VLA_Tutorials

¹⁷ <https://science.nrao.edu/facilities/vla/observing/callist#section-0>

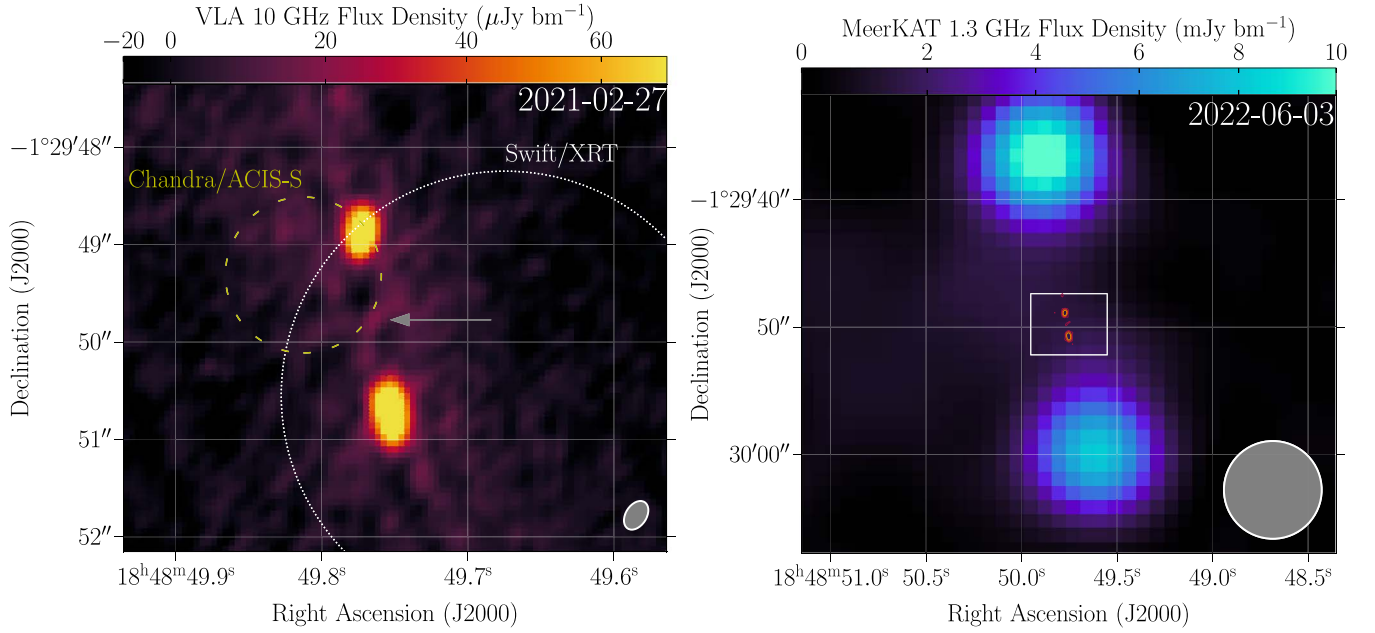


Figure 1. Left: VLA 10 GHz image of MAXI J1848–015 as observed on 2021 February 27. Two bright lobes are clearly detected. At the midpoint between the two lobes, a low-significance source (at 3.5σ) is present (denoted by a gray arrow). We demonstrate the motion of these lobes in Section 3.2. The white dashed circle indicates the localization of the X-ray transient by Kennea et al. (2021) based on Swift/XRT, while the yellow dotted circle represents the localization by Chakrabarty et al. (2021) based on Chandra/ACIS (both plotted with 90% confidence localization radii). The VLA synthesized beam is represented with a filled gray ellipse in the corner of the image. Right: MeerKAT 1.3 GHz image of outflows from MAXI J1848–015 as observed on 2022 June 3 (as an example for comparison with the VLA image on the left). The MeerKAT synthesized beam is represented with a filled gray ellipse in the corner of the image. The white box in the center indicates the region shown in the left panel and the red/orange contours are representative of the VLA flux densities on 2021 February 27 as shown in the left panel (representing 15, 30, and 60 μJy , from red to yellow). Note that the two panels have different spatial and flux density scales.

Briggs weighting with robust parameter 0 (to balance sensitivity and resolution), two Taylor terms to account for the wide fractional bandwidth, the multiscale algorithm (deconvolving with Gaussians of FWHM 5 and 15 pixels, as well as point sources), and placed an outlier field on a bright source to the south of our target.¹⁸ A zoomed-in image of the target is displayed in Figure 1 (left panel), where we clearly detect two bright radio lobe structures and potentially see indications of a weak (at 3.5σ significance) core component midway between the lobes (see Section 3.1).

2.2. MeerKAT

The field of MAXI J1848–015 was first observed with MeerKAT on 2021 February 28 (MJD 59,273) as part of The HUNT for Dynamic and Explosive Radio transients with MeerKAT (ThunderKAT¹⁹; Fender et al. 2017) large survey project. Following the radio detection of MAXI J1848–015 (Tremou et al. 2018), we observed the field weekly for 15 minutes of on-source integration time. Due to the slow evolution of the outflows, in 2021 October we decreased the observations and reduced the monitoring cadence to biweekly (for a total of 54 observations). Our observations were made using the *L*-band receiver, centered at 1.284 GHz with a bandwidth of 0.856 GHz. Observations typically alternated between the target and phase calibrator (J1911–2006), with a single scan on a bandpass and flux calibrator, J1939–6342. All observations were obtained in full polarization mode. We flagged the data using TRICOLOUR (Hugo et al. 2022) and calibrated the data using CASA as part of the OXKAT data

reduction scripts (Heywood 2020). For imaging the field of MAXI J1848–015, we used WSCLEAN (Offringa et al. 2014). The image size was $10,240 \times 10,240$ pixels, the pixel size was set at $1''.1$, and we used Briggs weighting with a robust parameter of -0.6 . We used the CASA task *imfit* to extract the flux densities and the positions of the two lobes. The two components were separated significantly, and a Gaussian fit (constrained to the size of the synthesized beam) was applied at each ejection component. We also account for 10% of the synthesized beam as a positional error.

3. Analysis and Results

3.1. Initial Identification of Moving Lobes and a Possible Compact Core

Our first radio observation of MAXI J1848–015, performed by the VLA on 2021 February 27, revealed two bright sources with flux densities of 256 ± 11 (“northern lobe”) and $176 \pm 6 \mu\text{Jy}$ (“southern lobe”) near the reported position of the system in the X-rays (Figure 1, left), with coordinates

$$\begin{aligned} \text{Northern lobe: } \text{R.A. (ICRS)} &= 18^{\text{h}} 48^{\text{m}} 49^{\text{s}}.7729 \pm 0.002, \\ \text{Decl. (ICRS)} &= -01^{\circ} 29' 48''.886 \pm 0.03 \\ \text{Southern lobe: } \text{R.A. (ICRS)} &= 18^{\text{h}} 48^{\text{m}} 49^{\text{s}}.7532 \pm 0.002, \\ \text{Decl. (ICRS)} &= -01^{\circ} 29' 50''.725 \pm 0.03. \end{aligned}$$

As we discuss below in Section 3.2, our follow-up MeerKAT monitoring campaign allowed us to establish that these two are outward-moving lobes. Both of these sources appear partially resolved when compared to the synthesized beam, indicating expansion of the outflows.

In addition to the bright lobes, we also notice a faint source approximately halfway between the two lobes, with a flux

¹⁸ Likely, GPS5 031.243–0.110, a candidate ultracompact H II region (Becker et al. 1994).

¹⁹ <http://www.thunderkat.uct.ac.za/>

density of $17.6 \mu\text{Jy}$, corresponding to a significance of 3.5σ , when compared to the local noise rms of $5.0 \mu\text{Jy}$ (calculated from an annulus around the source). Coordinates of this faint source (as estimated from the VLA observation on 2021 February 27) are

Potential compact core:

$$\text{R.A. (ICRS)} = 18^{\text{h}} 48^{\text{m}} 49^{\text{s}}.7628 \pm 0.002,$$

$$\text{Decl. (ICRS)} = -01^{\circ} 29' 49''.758 \pm 0.03.$$

The location of this faint source is consistent with reported localizations of MAXI J1848–015 in the X-rays by Chandra/ACIS and Swift/XRT, indicating that it is likely the compact core of MAXI J1848–015. Thus, hereafter, we assume this to be the case.

3.2. Modeling the Motion of the Outflows

The VLA in its most extended A-configuration provides a resolution (the FWHM of the synthesized beamwidth) of $\sim 0''.2$ at 10 GHz, whereas MeerKAT at 1.28 GHz provides a resolution of $\sim 6''$. Thus, while the lobes were already distinguishable in the VLA observation in 2021 February, it was not until 2021 April that the lobes were resolved by MeerKAT (Figure 2). Prior to this, MeerKAT only detected a single source with a flux density of ≈ 2 mJy at a location consistent with the X-ray and VLA positions of MAXI J1848–015. It is likely that this source is confused, as in addition to MeerKAT's inability to resolve the two sources at early times, contributions from pulsars, which can be abundant in globular clusters, may provide additional confusing sources at the frequency and resolution of our MeerKAT observations. The subsequent brightening of the lobes as they rose to a peak of ~ 50 mJy (Figure 2) led to distinguishable detection of the two lobes by MeerKAT and enabled us to track the motion of the lobes and constrain their properties. A full analysis of the flux density evolution of the lobes will be presented in E. Tremou et al. (2023, in preparation).

We model the outflowing lobes with a kinematic model along their direction of motion, comprising proper motion with constant deceleration and eventually stalling at zero velocity. To do so, we first apply the following coordinate transformation to the location of the lobes in each observation:

$$\begin{bmatrix} \theta_{\perp}^{N,i} \\ \theta_{\parallel}^{N,i} \end{bmatrix} = \begin{bmatrix} \cos \phi & -\sin \phi \\ \sin \phi & \cos \phi \end{bmatrix} \begin{bmatrix} \alpha^{N,i} - \alpha^0 \\ \delta^{N,i} - \delta^0 \end{bmatrix}, \quad (1)$$

where α and δ are R.A. and decl., with $[\alpha^{N,i}, \delta^{N,i}]$ representing coordinates of the northern lobe in each individual observation i . $[\alpha^0, \delta^0]$ represents the coordinates of the compact core, and ϕ is the jet axis on the sky plane—the angle between the lobes as initially measured in the first VLA observation (9.1° eastward from north in the equatorial coordinate system; Section 3.1). This transformation yields the displacement of the lobes as a combination of a component parallel to the jet axis ($\theta_{\parallel}^{N,i}$) and one perpendicular to that axis ($\theta_{\perp}^{N,i}$), allowing a simple ballistic modeling of the motion along the jet axis. An identical transformation is applied to the coordinates of the southern lobe in each observation. This transformation allows us to track the motions of the lobes along the jet axis while limiting the influence of any potential scatter as the lobes expand and their

weighted mean position becomes dominated by any hot spots. Such a scatter is expected, given the resolved nature of the lobes in our initial VLA epoch. While they may remain unresolved by MeerKAT, their measured positions will be a weighted mean of the emission, which could be biased by a hot spot in an expanding lobe (E. Tremou et al. 2023, in preparation).

With the transformed coordinates, we introduce the following model:

$$\theta_{\parallel}^N(t) = \begin{cases} \mu_{0,N}(t - t_0) + \frac{\dot{\mu}_N}{2}(t - t_0)^2 & t < t_{N,\text{stop}} \\ \mu_{0,N}(t_{N,\text{stop}} - t_0) + \frac{\dot{\mu}_N}{2}(t_{N,\text{stop}} - t_0)^2 & t \geq t_{N,\text{stop}} \end{cases} \quad (2)$$

$$\theta_{\parallel}^S(t) = \begin{cases} \mu_{0,S}(t - t_0) + \frac{\dot{\mu}_S}{2}(t - t_0)^2 & t < t_{S,\text{stop}} \\ \mu_{0,S}(t_{S,\text{stop}} - t_0) + \frac{\dot{\mu}_S}{2}(t_{S,\text{stop}} - t_0)^2 & t \geq t_{S,\text{stop}} \end{cases} \quad (3)$$

where $\mu_{0,S}$ and $\mu_{0,N}$ are proper motions at launch, t_0 is launch time, $\dot{\mu}_S$ and $\dot{\mu}_N$ are decelerations, and $t_{N,\text{stop}} = t_0 - \mu_{0,N}/\dot{\mu}_N$ and $t_{S,\text{stop}} = t_0 - \mu_{0,S}/\dot{\mu}_S$ are the times when the lobes stall completely due to deceleration. Given that the localizations of the northern and southern lobes are determined independently and that the lobes potentially move through different environments, we implement this model of motion with the normal likelihood

$$\begin{aligned} & p(\theta_{\parallel}^{N,i}, \theta_{\parallel}^{S,i} | \mu_{0,N}, \dot{\mu}_N, \mu_{0,S}, \dot{\mu}_S, \theta_{\text{scatter}}, t_0) \\ & = \mathcal{N}(\theta_{\parallel}^{N,i} | \theta_{\parallel}^N(t_i), \sigma^{N,i}) \mathcal{N}(\theta_{\parallel}^{S,i} | \theta_{\parallel}^S(t_i), \sigma^{S,i}), \end{aligned}$$

where \mathcal{N} denotes a normal probability density function, t_i is the time of the observation i , and

$$\sigma^{N,i} = \sqrt{(\sigma_{\theta_{\parallel}}^{N,i})^2 + (\theta_{\parallel}^{N,i} \tan \theta_{\text{scatter}})^2} \quad (4)$$

$$\sigma^{S,i} = \sqrt{(\sigma_{\theta_{\parallel}}^{S,i})^2 + (\theta_{\parallel}^{S,i} \tan \theta_{\text{scatter}})^2}. \quad (5)$$

Here, $\sigma_{\theta_{\parallel}}^{N,i}$, $\sigma_{\theta_{\parallel}}^{S,i}$ are the statistical uncertainties on localizations of the lobes in the θ_{\parallel} component. The second term considers an additional localization uncertainty caused by the expansion of the lobes, characterized by θ_{scatter} , which is the scatter angle as measured from the core along the jet axis (Figure 3, left). In our model we assume that the motion of the northern and southern lobes are independent of each other in most aspects except the time of ejection (t_0) and the scatter angle (θ_{scatter}). Using the same scatter angle for both lobes implies that the expansion of the lobes is dictated by their initial conditions. We assumed uniform priors for all model parameters as tabulated in Table 2.²⁰ We performed inference using Hamiltonian Monte Carlo with No-U-turn sampling through PYMC (version 4.1.2; Hoffman & Gelman 2011; Salvatier et al. 2016). We verified chain convergence through the rank-normalized convergence diagnostic (Gelman & Rubin 1992; Vehtari et al. 2019), finding $\hat{R} < 1.0001$ for each model parameter. Model parameter posterior samples are visualized in Figure 4, with point and

²⁰ We also verified that other choices of uninformative or weakly informative priors (such as log-uniform priors on μ and $\dot{\mu}$, or broad Gaussian priors for θ_{scatter}) do not influence the results.

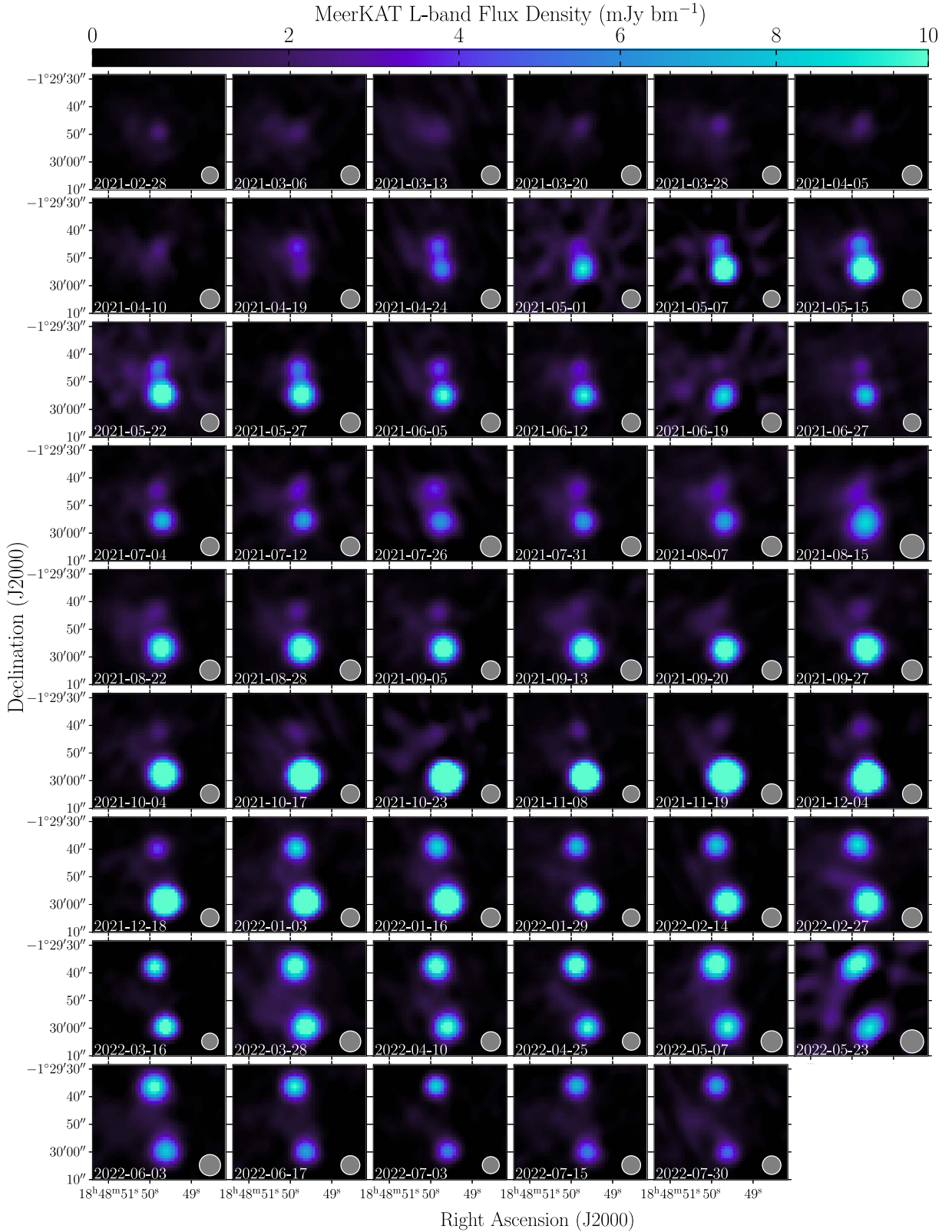


Figure 2. Detection and evolution of the outflows from MAXI J1848–015 as seen by MeerKAT (in the L band at 1.28 GHz), since it was first detected in 2021 February. Following the initial detection, both south and north lobes showed varying brightness. The two lobes were clearly distinguishable for the first time in 2021 April, approximately 2 months after the initial detection of the lobes by the VLA.

interval estimations reported in Table 2. The posterior sample median for θ_{scatter} is represented in Figure 3 (left), and the median and 90% highest density interval of the posterior models are plotted against the data in Figure 3 (right).

The model above allows us to estimate the initial proper motion of the lobes ($\mu_{0,N} = 33.1 \pm 1.4 \text{ mas d}^{-1}$ and $\mu_{0,S} = 48.1 \pm 2.1 \text{ mas day}^{-1}$), and provides a constraint on the possible outflow launch time ($59,246.4^{+2.4}_{-2.5} \text{ MJD}$,

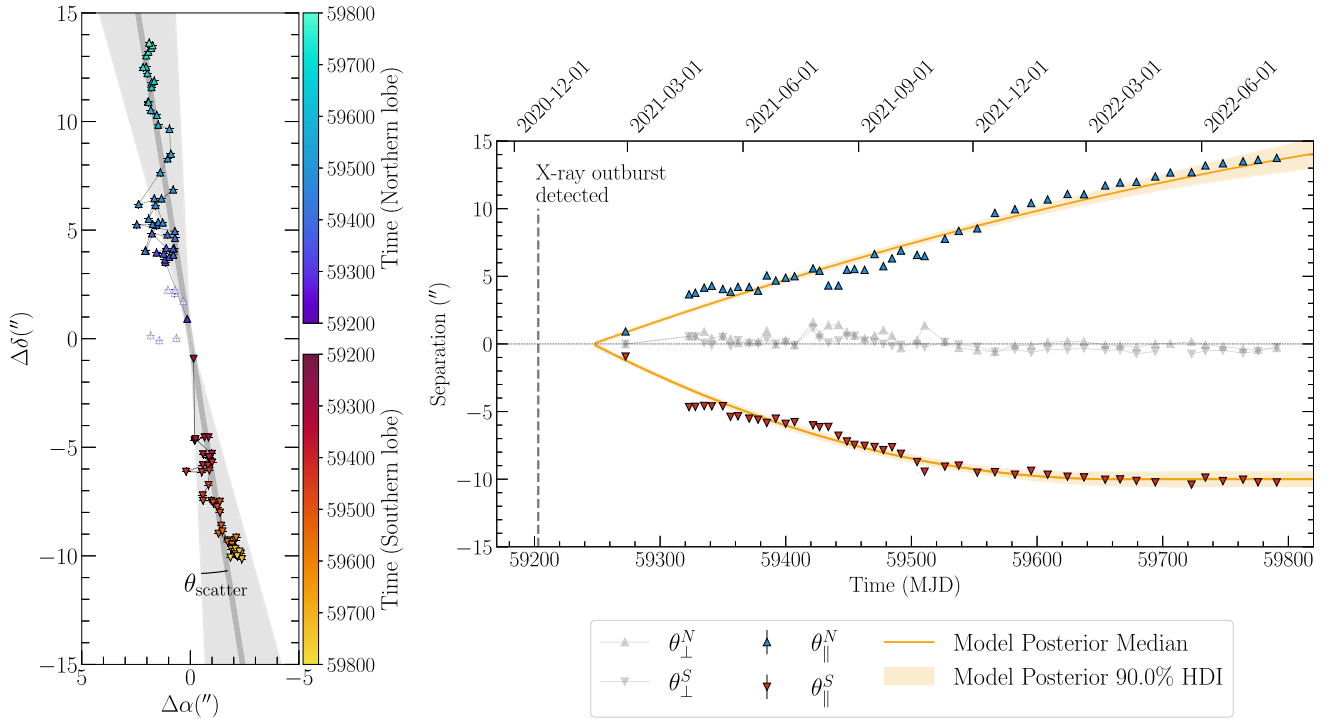


Figure 3. Left: position of the outflows from MAXI J1848–015 as observed over time. Unfilled markers represent observations in which the lobes could not be distinguished clearly. These observations were not included in the modeling. The gray line represents the jet axis on the sky plane as determined by the location of the lobes in the first VLA observation. The shaded gray interval represents the scatter angle (posterior median) as determined by our model (Section 3.2). Right: proper motion of the radio lobes parallel to the jet axis (colored triangles) and perpendicular to the jet axis (gray triangles), over time as observed during our monitoring campaign (error bars are smaller than the markers). The yellow line indicates a best-fit model, based on posterior medians, and the shaded yellow interval represent the 90% highest density interval of model posteriors.

Table 2

Prior Assumptions and Posterior Estimates for Model Parameters

Parameter	Prior	Posterior Estimates	\hat{R}
$\mu_{0,N}$ (mas day ⁻¹)	$\mathcal{U}(0, 1000)$	33.1 ± 1.4	1.00004
$\dot{\mu}_N$ (10 ⁻² mas day ⁻²)	$\mathcal{U}(-1000, 0)$	-3.0 ± 0.8	1.00006
$\mu_{0,S}$ (mas day ⁻¹)	$\mathcal{U}(-1000, 0)$	-48.1 ± 2.1	1.00006
$\dot{\mu}_S$ (10 ⁻² mas day ⁻²)	$\mathcal{U}(0, 1000)$	$11.6^{+1.3}_{-1.2}$	1.00007
θ_{scatter} (°)	$\mathcal{U}(0, 90)$	$6.5^{+0.6}_{-0.5}$	1.00003
t_0 (MJD)	$\mathcal{U}(59100, 59300)$	$59246.4^{+2.4}_{-2.5}$	1.00002

Note. All priors were assumed uniform (\mathcal{U}) with limits set to physically meaningful boundaries. The choice of prior for t_0 is to encompass the interval from before the detection of the X-ray outburst to after the first detection of the two lobes. Reported posterior estimates are median, 0.16, and 0.84 quantiles. \hat{R} is the rank-normalized convergence diagnostic (Gelman & Rubin 1992; Vehtari et al. 2019) to allow assessment of chain convergence.

corresponding to 2021 February 1). The inferred launch date suggests the launch of outflows may have occurred $43.1^{+2.4}_{-2.5}$ days after the discovery of the X-ray outburst on 2021 December 20. These constraints now enable us to explore intrinsic properties of the outflows and accretion in MAXI J1848–015.

It is worth noting that, as shown in Figure 3 (right), the model fails to explain the positional scatter of the lobes as observed by MeerKAT between \sim MJD 59,300 and 59,550. This scatter cannot be described by any simple model that does not account for effects such as energy injection or systematic effects such as uncertain localization of the marginally resolved lobes due to the presence of hot spots. Thus, it is likely that the

statistical uncertainty in the launch date inferred from our model is underestimated. It is also difficult to compare our inferred jet launch date with the date of any contemporaneous X-ray state transition, as MAXI J1848–015 spent a large fraction of its outburst in Sun constraint for many X-ray observatories.

4. Discussion

4.1. Distance to MAXI J1848–015 and Its Association with GLIMPSE-C01

In order to interpret the proper motions estimated above, we need to constrain the distance to MAXI J1848–015. First, we can obtain an upper limit on the distance using our estimates of the initial proper motions of the lobes ($\mu_{0,N}$, $\mu_{0,S}$), using the constraint that they cannot intrinsically be moving faster than the speed of light (e.g., Fender et al. 1999; Fender 2006). Using the posterior samples discussed in Section 3.2, we obtain an upper limit of $d_{\text{max}} = 4.3 \pm 0.2$ kpc, which rules out most of the Galactic bulge.

Second, while GLIMPSE-C01 is within the Galactic plane (located at ~ 3.4 kpc; Hare et al. 2018), with most of the Galactic stellar mass in this direction behind it, the fractional density of XRBs in globular clusters per unit stellar mass is ~ 150 times higher than in the rest of the Galaxy (e.g., Clark 1975; Heinke et al. 2003).

Thus, while the probability of a chance coincidence—and that MAXI J1848–015 could be behind GLIMPSE-C01—might have been worth considering in the absence of any other independent constraints; the presence of a tight maximum

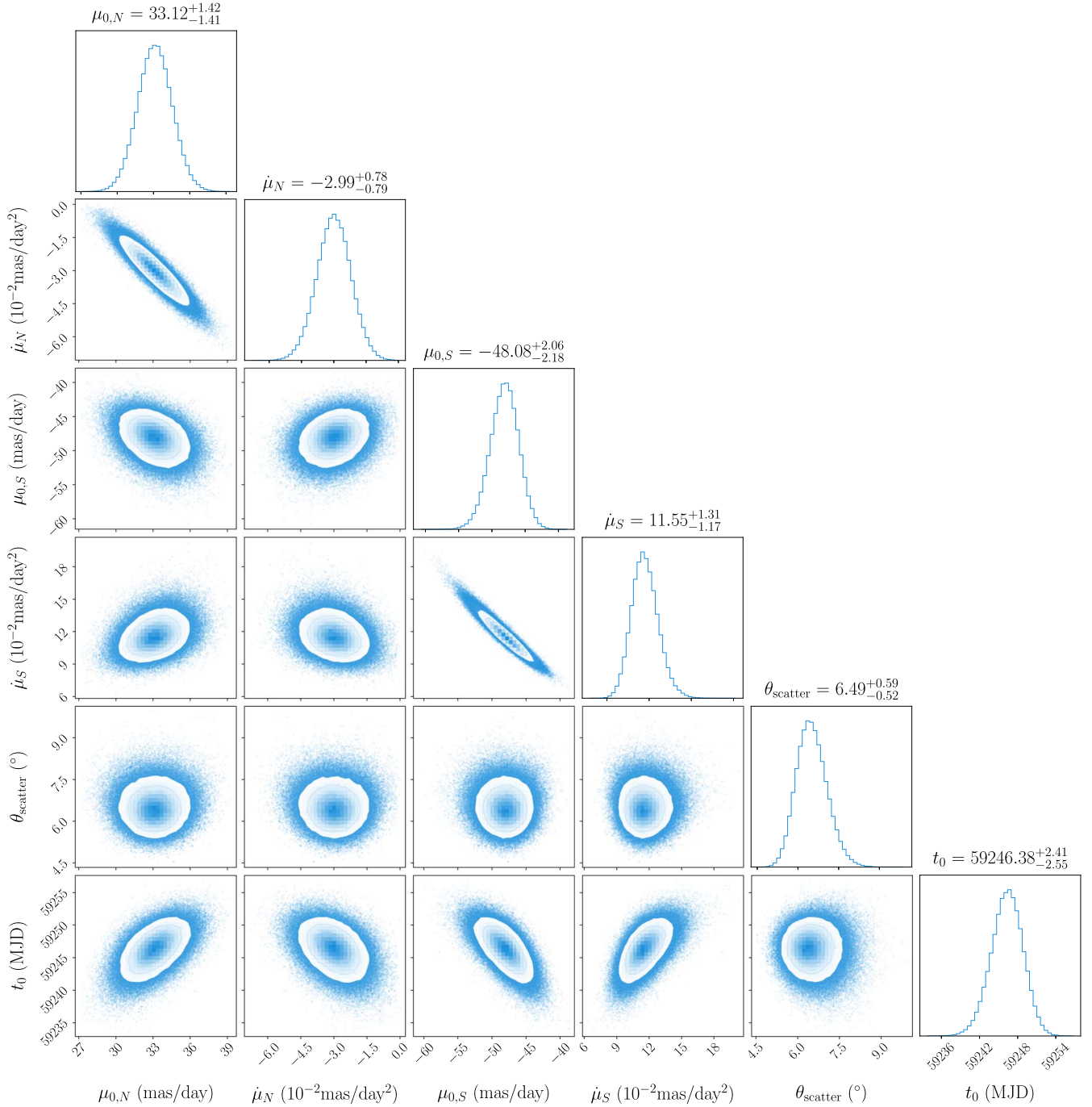


Figure 4. Pairwise plots of the posterior samples for parameters in the model described in Section 3.2. All samples appear unimodal. Significant anticorrelations are noticeable between proper motions and decelerations of the lobes. This is expected as with a lower initial proper motion; less deceleration would be needed to achieve a similar displacement. Initial proper motions and decelerations also show some degree of (anti)correlation with the predicted outflow launch date. This is likely due to the fact that the very early behavior of the outflows is only captured by a single highly influential observation (the VLA observation in 2021 February; see Figure 3).

distance constraint that rejects distances $\gtrsim 5$ kpc makes this probability negligible.

In addition, we should then consider whether MAXI J1848–015 could be a foreground object, in front of GLIMPSE-C01. While this possibility cannot be ruled out, it is still an unlikely scenario, as there is comparatively little stellar mass in this direction in front of GLIMPSE-C01.

Therefore, we conclude that MAXI J1848–015 is likely located within GLIMPSE-C01, at a distance of 3.4 ± 0.3 kpc as estimated by Hare et al. (2018). Hare et al. (2018) estimate the distance to GLIMPSE-C01 based on identification of red clump

stars in infrared observations. Given the high levels of extinction and crowding, they perform multiple iterations on selection and provide an estimate of 3.3–3.5 kpc, with a more conservative interval of 3.0–3.7 kpc. Thus, based on their work, here we conservatively assume a distance of 3.4 ± 0.3 kpc.

4.2. A Relativistic Outflow from a Globular Cluster XRB and Implications on the Accretion Properties

Using the constraints on initial proper motions of the lobes ($\mu_{0,N}$, $\mu_{0,S}$), and assuming that the outflows are intrinsically

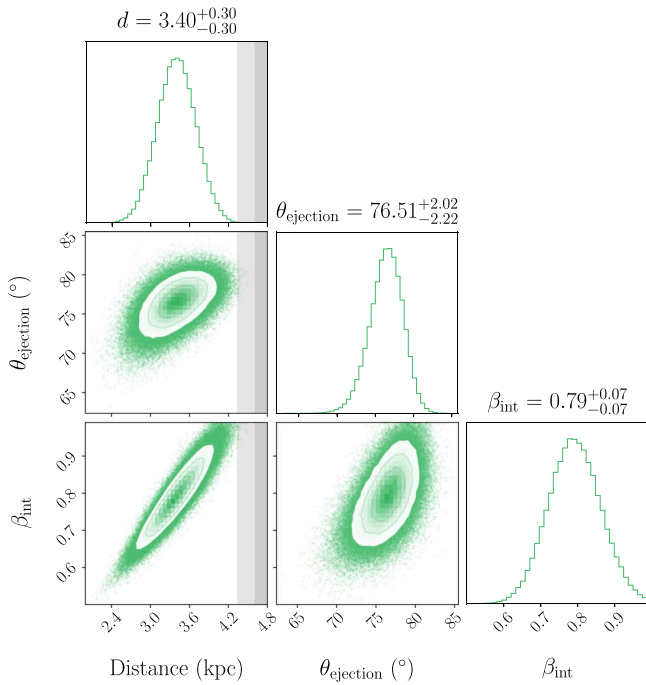


Figure 5. Pairwise plots for the ejection angle and the intrinsic speed of ejection ($\beta_{\text{int}} = v/c$, where c is speed of light), estimated using the posterior samples for $\mu_{0,N}$ and $\mu_{0,S}$, and assuming a distance of 3.4 ± 0.3 kpc (Hare et al. 2018). The shaded light and dark gray intervals in the pairwise panels containing distance indicate the median and 95% quantile, respectively, on the maximum possible distance as inferred in Section 4.1.

symmetric, we can estimate the angle of ejection to the line of sight (θ_{ejection}) and the intrinsic velocity of the lobes ($\beta_{\text{int}} = v/c$) following Rees (1966), Blandford et al. (1977), Mirabel & Rodríguez (1994), and Fender (2006). For this purpose, we use our posterior samples for $\mu_{0,N}$ and $\mu_{0,S}$ and estimate $\beta_{\text{int}} \cos \theta_{\text{ejection}} = 0.19 \pm 0.02$. Following that, with a randomly generated sample of distance values assuming a normal probability density function for distance with a mean of 3.4 kpc and a standard deviation of 0.3 kpc (see Section 4.1), we estimate $\theta_{\text{ejection}} = 77^\circ \pm 2^\circ$ and subsequently $\beta_{\text{int}} = 0.79 \pm 0.07$ (Figure 5).

If we assume there is no significant misalignment between the jet and accretion disk (but see Maccarone 2002), the inferred θ_{ejection} indicates a high inclination angle. A high inclination angle would be in tension with the inclination angle of the inner accretion disk estimated by Pike et al. (2022), who used X-ray spectral modeling to infer a low inclination angle of $\approx 26.4 \pm 0.5^\circ$ for the inner accretion disk. This tension may indicate that there is a high degree of disk–jet misalignment in MAXIJ1848–015. However, we note that a high inclination angle would help explain the apparently low X-ray luminosity of the outburst states observed in this system (as highlighted by Pike et al. 2022) through obscuration.

Additionally, Pike et al. (2022) indicate that while their modeling is not particularly sensitive to the inclination of the outer disk, when left to vary independently, it yields a suggestive value of $79^{+6}_{-11}^\circ$. This may suggest that the accretion disk could be warped. If this is indeed the case, the potential alignment between the jet and the outer accretion disk (while the inner disk is misaligned with both) may be indicative of the influence of the outer disk on outflow launching in XRBs (e.g., Liska et al. 2019).

Our inferred values of the initial proper motions (≈ 34 and 50 mas day $^{-1}$) and intrinsic jet speed $\beta_{\text{int}} = 0.79 \pm 0.07$ indicate a relatively slow moving outflow for MAXIJ1848–015 as compared to some other XRBs. For example, outflows from GRS 1915+105 (Mirabel & Rodríguez 1994; Fender et al. 1999), GRO J1655–40 (Hjellming & Rupen 1995), XTE J1550–564 (Corbel et al. 2002), GX 339–4 (Gallo et al. 2004), XTE J1550–564 (Hannikainen et al. 2009), MAXIJ1535–571 (Russell et al. 2019), MAXIJ1820+070 (Bright et al. 2020), and MAXIJ1348–630 (Carotenuto et al. 2021) have been observed to be faster, and relatively close to the speed of light.²¹ In contrast, systems such as SS 433 (Fabian & Rees 1979), XTE J1752–223 (Yang et al. 2010; Miller-Jones et al. 2011), XTE J1908+094 (Rushton et al. 2017), V404 Cygni (Miller-Jones et al. 2019), and EXO 1846–031 (Williams et al. 2022) have shown slower-moving outflows, with speeds comparable to MAXIJ1848–015, as estimated in this work. In addition, among the large-scale outflows from XRBs, those observed in MAXIJ1848–015 have propagated a relatively small distance at a slow apparent speed—e.g., in contrast with MAXIJ1820+070, MAXIJ1348–630, XTE J1550–564, and MAXIJ1535–571. However, some XRBs have been observed to decelerate on smaller angular scales (e.g., XTE J1752–223, EXO 1846–031; Miller-Jones et al. 2011; Williams et al. 2022).

Finally, it is worth noting that Pike et al. (2022) detected evolving narrow Fe emission lines in their observations of MAXIJ1848–015 in 2020 December—considerably earlier than our first detection of the outflows at the end of 2021 February, or the projected outflow launch inferred from our model, at the beginning of 2021 February. They discuss jet launching as one possible scenario for the origin of these lines. While we might have found the jets predicted by Pike et al. (2022), the timeline of events suggests that there could potentially have been multiple jet-launching events. However, we find no evidence for multiple sets of jet knots in either the VLA or the MeerKAT observations. In particular, we imaged the VLA observation out to 4/5 (the FWHM of the VLA primary beam at 10 GHz) and searched along the jet propagation axis for evidence of ejecta that may have been launched earlier than the lobes detected in the VLA observation (Figure 1, left), and we found no evidence for the presence of such ejecta.

4.3. Nature of the System and the Compact Object

The likely presence of MAXIJ1848–015 in a globular cluster indicates that it is a low-mass XRB (as opposed to a high-mass XRB). Based on its X-ray temporal and spectral properties, particularly the broad Fe line, Pike et al. (2022) speculate that the compact object in this system may be a black hole—while determining the nature of the compact object in XRBs using such features can be uncertain.

Our observations of strong outflows from MAXIJ1848–015 also hint at a black hole nature, as similarly powerful (i.e., bright and moving at relativistic speeds) outflows are more commonly seen from accreting black holes than from neutron star systems. However, we cannot conclusively rule out a neutron star nature, as accreting neutron stars with powerful

²¹ It is worth noting that the distance to many of these systems is not well constrained and very few have measured parallaxes. This can influence estimated intrinsic velocities significantly (Fender et al. 2003).

outflows have also been observed—albeit, much less frequently than black holes. For example, such outflows have been seen from the neutron star XRBs Circinus X-1 (Fender et al. 2004; Tudose et al. 2008) and Scorpius X-1 (Fomalont et al. 2001a, 2001b), although both these sources differ from MAXIJ1848–015 in some of their key characteristics. Circinus X-1 is a very young (~ 5 kyr; Heinz et al. 2013) neutron star high-mass XRB system, which are not found in old star clusters. Scorpius X-1 is an neutron star low-mass XRB persistently accreting at close to the Eddington luminosity (in contrast to the transient nature of MAXIJ1848–015). While it has shown bright relativistic outflows, at their brightest these were ~ 1 order of magnitude fainter than the outflows observed in MAXIJ1848–015 at their brightest, despite the distances being comparable.

We detect faint radio emission from a putative compact core (Section 3.1). Considering the disk–jet coupling in accreting systems (Fender et al. 2003; Bahramian & Rushton 2022), the VLA detection and the Swift/XRT observation performed on the same day as the VLA observation would place MAXIJ1848–015 below both the black hole tracks and the vast majority of neutron star systems ($L_R \approx 3 \times 10^{26}$ erg s $^{-1}$, and an apparent $L_X \approx 10^{35}$ erg s $^{-1}$). However, the X-ray spectrum of that observation and the one performed a few days earlier and reported by Kennea et al. (2021) both indicate a rather soft spectrum (power-law photon index ≥ 2), which suggest that the source was not in a hard state at the time, and thus it would be inappropriate to place it on the radio/X-ray plane. The high inclination angle also can lead to underestimation of the X-ray luminosity, making the source even more underluminous in the radio.²²

Thus, while our observations of the outflows from MAXIJ1848–015 indicate a behavior consistent with previously observed black hole candidate low-mass XRBs, the nature of the compact object in this system cannot be definitively confirmed.

It is worth noting that if MAXIJ1848–015 does host a black hole, it would be among the very small sample of black holes identified in globular clusters. While globular clusters are expected to produce a large population of black holes through stellar evolution, almost all of these black holes are expected to escape the cluster over a rather short period of time (Sigurdsson & Hernquist 1993). However, the presence of black holes in globular clusters has recently been confirmed through detection of dynamically confirmed “detached” (nonaccreting) black holes in NGC 3201 (Giesers et al. 2018, 2019).

To date, there have been no dynamically confirmed black hole XRBs identified in any globular cluster, although over the past two decades, a handful of candidates have been identified in Galactic and extragalactic globular clusters (e.g., see Maccarone et al. 2007; Strader et al. 2012; Chomiuk et al. 2013; Miller-Jones et al. 2015; Shishkovsky et al. 2018; Dage et al. 2019, 2020). All the Galactic candidates among these have been identified in quiescent/faint states ($L_X \leq 10^{34}$ erg s $^{-1}$) and none have so far shown bright ($L_X \geq 10^{35}$ erg s $^{-1}$) outbursts. In contrast, almost all the currently known bright persistent and transient Galactic globular cluster XRBs have been confirmed to contain neutron stars (see Bahramian & Degenaar 2022, Table 7). Thus, MAXIJ1848–015 may be the

first outbursting black hole XRB identified in a Galactic globular cluster.

5. Conclusion

In this work we presented results of our radio monitoring of the outburst of MAXIJ1848–015 and report the first detection of expanding and decelerating outflows from an XRB in a globular cluster. Using the MeerKAT observatory, we monitored large-scale outflows from MAXIJ1848–015 regularly for over 500 days, obtaining an extraordinary coverage of such outflows. Using a kinematic model, we constrain initial proper motion of the outflows and constrain the possible launch date. We find $\beta_{\text{int}} \cos \theta_{\text{ejection}} = 0.19 \pm 0.02$. Assuming MAXIJ1848–015 is located in the globular cluster GLIMPSE-C01, at 3.4 kpc, we determine the intrinsic jet speed, $\beta_{\text{int}} = 0.79 \pm 0.07$, and the inclination angle to the line of sight, $\theta_{\text{ejection}} = 76^\circ \pm 2^\circ$. Additionally, the estimated proper motions in our modeling imply a maximum possible distance of 4.3 ± 0.2 kpc and indicate comparatively slow moving outflows in contrast with XRBs that have been observed with outflows. Our findings also provide additional circumstantial evidence indicating MAXIJ1848–015 could be a black hole XRB, which if confirmed would make it the first such system in a globular cluster to show a transient outburst.

A.B. thanks Eric W. Koch for helpful discussions. A.J.T. acknowledges support for this work was provided by NASA through the NASA Hubble Fellowship grant #HST-HF2–51494.001 awarded by the Space Telescope Science Institute, which is operated by the Association of Universities for Research in Astronomy, Inc., for NASA, under contract NAS5–26555. F.C. acknowledges support from the Royal Society through the Newton International Fellowship program (NIF/R1/211296). J.S. acknowledges support from NASA grant 80NSSC21K0628 and the Packard Foundation.

The MeerKAT telescope is operated by the South African Radio Astronomy Observatory, which is a facility of the National Research Foundation, an agency of the Department of Science and Innovation. We acknowledge the use of the Inter-University Institute for Data Intensive Astronomy (IDIA) data intensive research cloud for data processing. IDIA is a South African university partnership involving the University of Cape Town, the University of Pretoria and the University of the Western Cape.




We thank the VLA director and staff for accommodating our DDT request. The National Radio Astronomy Observatory is a facility of the National Science Foundation operated under cooperative agreement by Associated Universities, Inc. We acknowledge extensive use of NASA’s Astrophysics Data System Bibliographic Services, arXiv, and SIMBAD (Wenger et al. 2000).

Facilities: VLA, MeerKAT.

Software: Astropy (Astropy Collaboration et al. 2013, 2018), CASA (THE CASA TEAM et al. 2022) Corner (Foreman-Mackey 2016), IPython (Perez & Granger 2007), Jupyter (Kluyver et al. 2016), Matplotlib (Hunter 2007), Numpy (Oliphant 2006; van der Walt et al. 2011), PyMC (Salvatier et al. 2016), SAOImage DS9 (Joye & Mandel 2003), Scipy (Virtanen et al. 2020).

²² For an example of how inclination angle affects the disk–jet coupling diagnostics, see the discussion on GRS 1747–312 in Panurach et al. (2021).

ORCID iDs

A. Bahramian  <https://orcid.org/0000-0003-2506-6041>
 E. Tremou  <https://orcid.org/0000-0002-4039-6703>
 A. J. Tetarenko  <https://orcid.org/0000-0003-3906-4354>
 J. C. A. Miller-Jones  <https://orcid.org/0000-0003-3124-2814>
 S. Corbel  <https://orcid.org/0000-0001-5538-5831>
 D. R. A. Williams  <https://orcid.org/0000-0001-7361-0246>
 J. Strader  <https://orcid.org/0000-0002-1468-9668>
 F. Carotenuto  <https://orcid.org/0000-0002-0426-3276>
 R. Salinas  <https://orcid.org/0000-0002-1206-1930>
 J. A. Kennea  <https://orcid.org/0000-0002-6745-4790>
 S. E. Motta  <https://orcid.org/0000-0002-6154-5843>
 P. A. Woudt  <https://orcid.org/0000-0002-6896-1655>
 J. H. Matthews  <https://orcid.org/0000-0002-3493-7737>
 T. D. Russell  <https://orcid.org/0000-0002-7930-2276>

References

- Astropy Collaboration, Price-Whelan, A. M., Sipőcz, B. M., et al. 2018, *AJ*, **156**, 123
- Astropy Collaboration, Robitaille, T. P., Tollerud, E. J., et al. 2013, *A&A*, **558**, A33
- Bahramian, A., & Degenaar, N. 2022, arXiv:2206.10053
- Bahramian, A., Heinke, C. O., Sivakoff, G. R., & Gladstone, J. C. 2013, *ApJ*, **766**, 136
- Bahramian, A., & Rushton, A. 2022, *bersavosh/XRB-LrLx_pub*: update 220808, Zenodo, doi:10.5281/zenodo.6972578
- Becker, R. H., White, R. L., Helfand, D. J., & Zoonematkermani, S. 1994, *ApJS*, **91**, 347
- Blandford, R. D., McKee, C. F., & Rees, M. J. 1977, *Natur*, **267**, 211
- Bright, J. S., Fender, R. P., Motta, S. E., et al. 2020, *NatAs*, **4**, 697
- Brocksopp, C., Miller-Jones, J. C. A., Fender, R. P., & Stappers, B. W. 2007, *MNRAS*, **378**, 1111
- Carotenuto, F., Corbel, S., Tremou, E., et al. 2021, *MNRAS*, **504**, 444
- Chakrabarty, D., Jonker, P. G., Homan, J., & van den Berg, M. 2021, *ATel*, **14424**, 1
- Chomiuk, L., Strader, J., Maccarone, T. J., et al. 2013, *ApJ*, **777**, 69
- Clark, G. W. 1975, *ApJL*, **199**, L143
- Corbel, S., Fender, R. P., Tzioumis, A. K., et al. 2002, *Sci*, **298**, 196
- Corbel, S., Kaaret, P., Fender, R. P., et al. 2005, *ApJ*, **632**, 504
- Corbel, S., Kaaret, P., Jain, R. K., et al. 2001, *ApJ*, **554**, 43
- Dage, K. C., Zepf, S. E., Bahramian, A., et al. 2019, *MNRAS*, **489**, 4783
- Dage, K. C., Zepf, S. E., Thygesen, E., et al. 2020, *MNRAS*, **497**, 596
- Davidge, T. J., Andersen, D. R., Lardière, O., et al. 2016, *AJ*, **152**, 173
- Fabian, A. C., Pringle, J. E., & Rees, M. J. 1975, *MNRAS*, **172**, 15P
- Fabian, A. C., & Rees, M. J. 1979, *MNRAS*, **187**, 13P
- Fender, R., Woudt, P. A., Corbel, S., et al. 2017, in *Proc. of MeerKAT Science: On the Pathway to the SKA*, **13**
- Fender, R., Wu, K., Johnston, H., et al. 2004, *Natur*, **427**, 222
- Fender, R. P., Gallo, E., & Jonker, P. G. 2003, *MNRAS*, **343**, L99
- Fender, R. P., Garrington, S. T., McKay, D. J., et al. 1999, *MNRAS*, **304**, 865
- Fender, R. 2006, *Compact stellar X-ray sources*, Vol. 39 (Cambridge: Cambridge Univ. Press), 381
- Fomalont, E. B., Geldzahler, B. J., & Bradshaw, C. F. 2001a, *ApJ*, **558**, 283
- Fomalont, E. B., Geldzahler, B. J., & Bradshaw, C. F. 2001b, *ApJL*, **553**, L27
- Foreman-Mackey, D. 2016, *JOSS*, **1**, 24
- Gallo, E., Corbel, S., Fender, R. P., Maccarone, T. J., & Tzioumis, A. K. 2004, *MNRAS*, **347**, L52
- Gelman, A., & Rubin, D. B. 1992, *StaSc*, **7**, 457
- Giesers, B., Dreizler, S., Husser, T.-O., et al. 2018, *MNRAS*, **475**, L15
- Giesers, B., Kamann, S., Dreizler, S., et al. 2019, *A&A*, **632**, A3
- Hannikainen, D. C., Hunstead, R. W., Wu, K., et al. 2009, *MNRAS*, **397**, 569
- Hare, J., Kargaltsev, O., & Rangelov, B. 2018, *ApJ*, **865**, 33
- Hare, J., Yang, H., Kargaltsev, O., et al. 2021, *ATel*, **14499**, 1
- Harris, W. E. 1996, *AJ*, **112**, 1487
- Heinke, C. O., Grindlay, J. E., Luger, P. M., et al. 2003, *ApJ*, **598**, 501
- Heinz, S., Sell, P., Fender, R. P., et al. 2013, *ApJ*, **779**, 171
- Heywood, I. 2020, *oxkat: Semi-automated imaging of MeerKAT observations*, Astrophysics Source Code Library, ascl:2009.003
- Hills, J. G. 1976, *MNRAS*, **175**, 1P
- Hjellming, R. M., & Rupen, M. P. 1995, *Natur*, **375**, 464
- Hoffman, M. D., & Gelman, A. 2011, arXiv:1111.4246
- Hugo, B. V., Perkins, S., Merry, B., Mauch, T., & Smirnov, O. M. 2022, in *ASP Conference Series*, 532, ed. J. E. Ruiz, F. Pierfederici, & P. Teuben (San Francisco, CA: ASP), 541
- Hunter, J. D. 2007, *CSE*, **9**, 90
- Ivanov, V. D., Kurtev, R., & Borisova, J. 2005, *A&A*, **442**, 195
- Joye, W. A., & Mandel, E. 2003, in *ASP Conf. Ser.* 295, ed. H. E. Payne, R. I. Jedrzejewski, & R. N. Hook (San Francisco, CA: ASP), 489
- Kennea, J. A., Bahramian, A., Evans, P. A., et al. 2021, *ATel*, **14420**, 1
- Kluuyver, T., Ragan-Kelley, B., Pérez, F., et al. 2016, in *Positioning and Power in Academic Publishing: Players, Agents and Agendas*, ed. F. Loizides & B. Schmidt (Amsterdam: IOS Press), 87
- Kobulnicky, H. A., Monson, A. J., Buckalew, B. A., et al. 2005, *AJ*, **129**, 239
- Kundu, A., Maccarone, T. J., & Zepf, S. E. 2007, *ApJ*, **662**, 525
- Kundu, A., & Zepf, S. E. 2007, *ApJL*, **660**, L109
- Liska, M., Tchekhovskoy, A., Ingram, A., & van der Klis, M. 2019, *MNRAS*, **487**, 550
- Maccarone, T. J. 2002, *MNRAS*, **336**, 1371
- Maccarone, T. J., Kundu, A., Zepf, S. E., & Rhode, K. L. 2007, *Natur*, **445**, 183
- Martí, J., Luque-Escamilla, P. L., Bosch-Ramon, V., & Paredes, J. M. 2017, *NatCo*, **8**, 1757
- Mihara, T., Negoro, H., Shidatsu, M., et al. 2021, *ATel*, **14327**, 1
- Miller-Jones, J. C. A., Jonker, P. G., Ratti, E. M., et al. 2011, *MNRAS*, **415**, 306
- Miller-Jones, J. C. A., Strader, J., Heinke, C. O., et al. 2015, *MNRAS*, **453**, 3918
- Miller-Jones, J. C. A., Tetarenko, A. J., Sivakoff, G. R., et al. 2019, *Natur*, **569**, 374
- Mirabel, I. F., & Rodríguez, L. F. 1994, *Natur*, **371**, 46
- Offringa, A. R., McKinley, B., Hurley-Walker, N., et al. 2014, *MNRAS*, **444**, 606
- Oliphant, T. E. 2006, *A guide to NumPy*, Vol. 1 (USA: Trelgol Publishing)
- Panurach, T., Strader, J., Bahramian, A., et al. 2021, *ApJ*, **923**, 88
- Perez, F., & Granger, B. E. 2007, *CSE*, **9**, 21
- Pike, S. N., Harrison, F. A., Forster, K., et al. 2020, *ATel*, **14290**, 1
- Pike, S. N., Negoro, H., Tomsick, J. A., et al. 2022, *ApJ*, **927**, 190
- Pooley, D., Lewin, W. H. G., Anderson, S. F., et al. 2003, *ApJL*, **591**, L131
- Pooley, D., Rappaport, S., Levine, A., Pfahl, E., & Schwab, J. 2007, arXiv:0708.3365
- Rees, M. J. 1966, *Natur*, **211**, 468
- Rushton, A. P., Miller-Jones, J. C. A., Curran, P. A., et al. 2017, *MNRAS*, **468**, 2788
- Russell, T. D., Tetarenko, A. J., Miller-Jones, J. C. A., et al. 2019, *ApJ*, **883**, 198
- Salvatier, J., Wiecki, T. V., & Fonnesbeck, C. 2016, *PeerJ Comput. Sci.*, **2**, e55
- Sarazin, C. L., Kundu, A., Irwin, J. A., et al. 2003, *ApJ*, **595**, 743
- Shishkovsky, L., Strader, J., Chomiuk, L., et al. 2018, *ApJ*, **855**, 55
- Sigurdsson, S., & Hernquist, L. 1993, *Natur*, **364**, 423
- Strader, J., Chomiuk, L., Maccarone, T. J., Miller-Jones, J. C. A., & Seth, A. C. 2012, *Natur*, **490**, 71
- Sutantyo, W. 1975, *A&A*, **44**, 227
- Takagi, R., Negoro, H., Serino, M., et al. 2020, *ATel*, **14282**, 1
- THE CASA TEAM, Bean, B., Bhatnagar, S., et al. 2022, *PASP*, **1041**, 114501
- Tremou, E., Strader, J., Chomiuk, L., et al. 2018, *ApJ*, **862**, 16
- Tudose, V., Fender, R. P., Tzioumis, A. K., Spencer, R. E., & van der Klis, M. 2008, *MNRAS*, **390**, 447
- van der Walt, S., Colbert, S. C., & Varoquaux, G. 2011, *CSE*, **13**, 22
- Vehtari, A., Gelman, A., Simpson, D., Carpenter, B., & Bürkner, P.-C. 2019, arXiv:1903.08008
- Virtanen, P., Gommers, R., Oliphant, T. E., et al. 2020, *NatMe*, **17**, 261
- Wenger, M., Ochsenbein, F., Egret, D., et al. 2000, *A&AS*, **143**, 9
- Williams, D. R. A., Motta, S. E., Fender, R., et al. 2022, *MNRAS*, **517**, 2801
- Yang, J., Brocksopp, C., Corbel, S., et al. 2010, *MNRAS*, **409**, L64
- Yang, J., Paragi, Z., Corbel, S., et al. 2011, *MNRAS*, **418**, L25